Convolutional Neural Networks Applied to 2D and 3D DC Resistivity Inversion

Sascha Weit[1], Ralph-Uwe Börner[1], Matthias Brändel[2], Peggy Gödickmeier[1], Richard Gootjes[2], Samuel Kost[2], Oliver Rheinbach[2], Mathias Scheunert[1], and Klaus Spitzer[1]

[1]*Institute of Geophysics and Geoinformatics, TU Bergakademie Freiberg*
[2]*Institute of Numerical Mathematics and Optimization, TU Bergakademie Freiberg*

1 Motivation

Geophysical Inversion is often very time consuming and requires previous knowledge on the geological environment of the survey area. Both of these factors could be avoided by utilizing neural networks for geophysical inversion. Distinguishing the effects of anomalies from the ones produced by a geologic background is very similar to an image segmentation approach. This approach is very established and has been shown to work in a variety of fields. Image segmentation is traditionally accomplished using convolutional neural networks. Here, we present an approach of utilizing convolutional neural networks for the task of regression applied to DC data. Network architecture, forward modelling and preliminary results will be discussed.

2 Architecture and Experimental Design

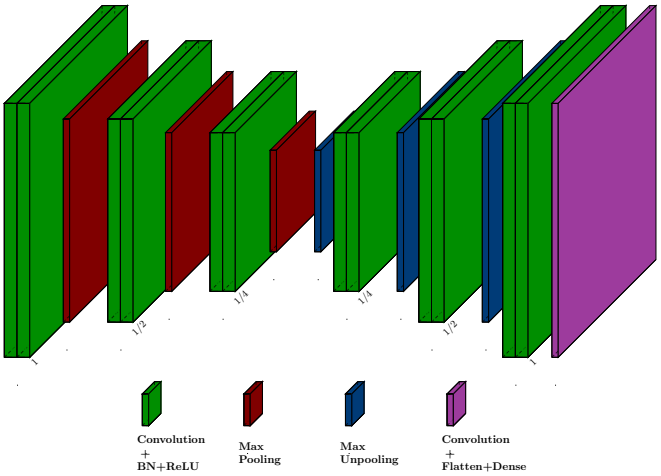

Figure 1: Architecture used for training 2D inversion

Architecture for segmentation often follows an encoder/decoder scheme (see Fig. 1. During the encoding, convolutional layers and MaxPooling layers are used to filter out the most

important information. This then gets transformed during the decoder step with the use of MaxUnpooling layers. The traditional SegNet architecture (Badrinarayanan et al., 2017) uses a varying number of pooling and unpooling layers, with a final Softmax layer for segmentation. Here, this architecture is slightly modified to perform regression by replacing the Softmax layer with a Dense layer (see Fig. 1). This also mirrors the approach to an architecture used by Vu and Jardani (2021). In the 3D case, the MaxUnpooling layer is replaced by a combination of UpSampling3D and Concatenate layers, effectively turning the network into a U-Net (Ronneberger et al., 2015). This decision was made due to the lack of an established MaxUnpooling3D layer. All training and evaluation was performed using the Keras API for Tensorflow (Abadi et al., 2016).
To attain the amount of data needed for training a neural network, synthetic DC data were generated. The synthetic forward modeling was performed using Matlab with an in-house finite element routine (Scheunert et al., 2021). We simulated DC measurements along 17 Profiles with 17 Electrodes each in a dipole-dipole configuration. The distance between profiles and electrodes was 3 m. This setup was deliberately chosen to compare results with Vu and Jardani (2021). 1-5 spherical anomalies were randomly placed below the central profile. Background resistivity was set to 4000 Ωm, anomaly resistivity was lower. An example with 3 spheres is shown in Fig. 2.

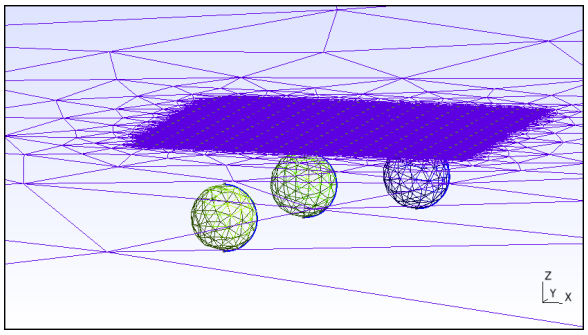

Figure 2: Mesh example for 3 spheres. Mesh is only shown on boundary surfaces.

The 17 pseudo sections were mapped onto a 32x32x16 grid with grid cells of the size 1.5m in every spatial direction (see Fig. 3 for one profile). Background resistivity was assumed for every cell not corresponding to a value from the pseudo section (again note Fig. 3).

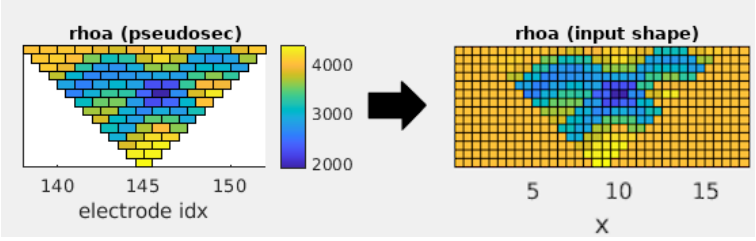

Figure 3: Mapping of a pseudo section to a 32x16 grid.

Input ρ_a and ρ were finally transformed before being supplied to the network:

$$\rho_{a,in} = 10(log_{10}(\rho_a) - 3.5) \tag{1}$$

$$\rho_{in} = log_{10}(\rho) \tag{2}$$

3 Results

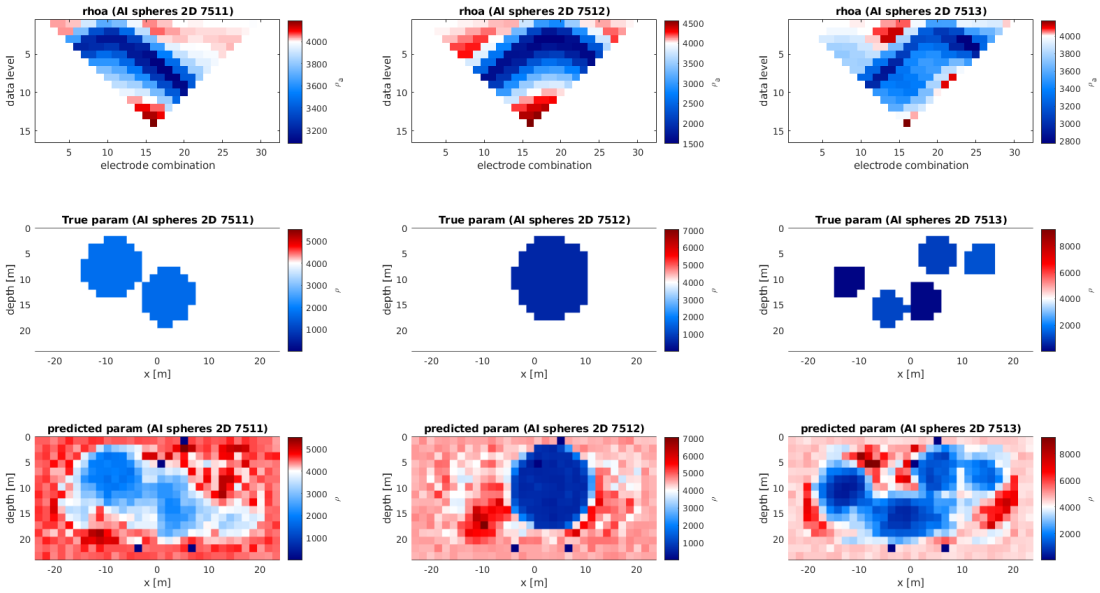

Figure 4: Training results for 2D data without noise. From top to bottom: Input ρ_a, ground truth (ρ), predicted ρ. From left to right represents 3 different cases.

Fig. 4 shows predictions for 3 different cases. No noise has been applied to this data set and data were 2D sections along the center profile taken from the 3D models. Prediction of anomaly resistivities and locations are close to the ground truth. Multiple spheres are often not recognized by the network as separate entities. The background resistivity is generally overestimated in the predictions. The prediction contains 4 dead pixels that are present in every case. This effect likely stems from over-training.

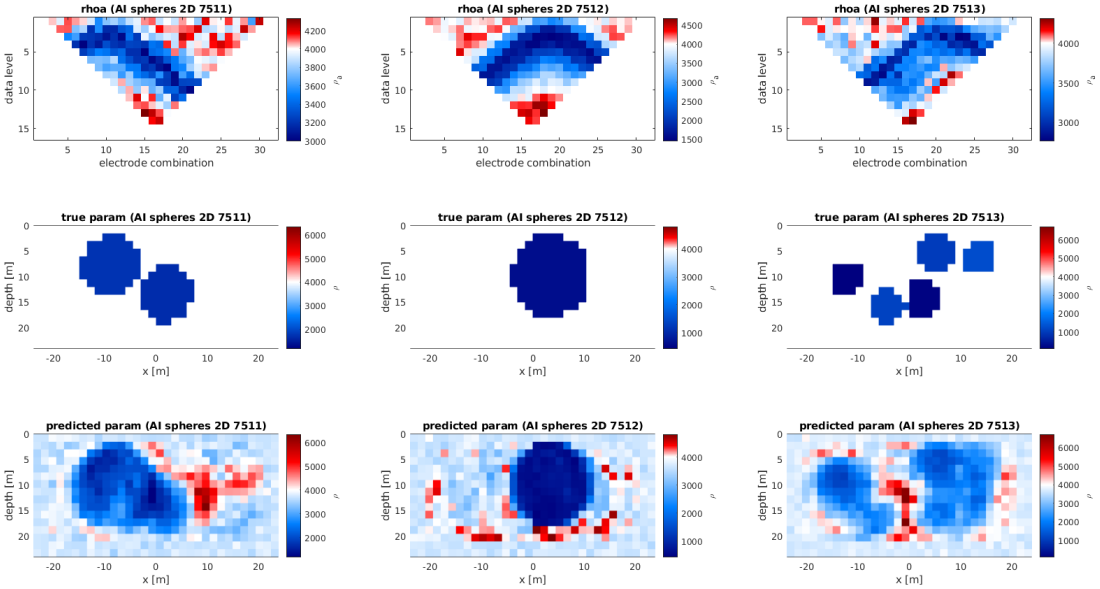

Figure 5: Training results for 2D data with noise. From top to bottom: Input ρ_a, ground truth (ρ), predicted ρ. From left to right represents 3 different cases.

Results for the 3D case show similar characteristics: The anomaly shape and resistivity is matched especially well for single, large anomalies. The background is generally overestimated, this time much more than in the 2D case. Resistivity and location of smaller anomalies are matched much more poorly in the 3D case.

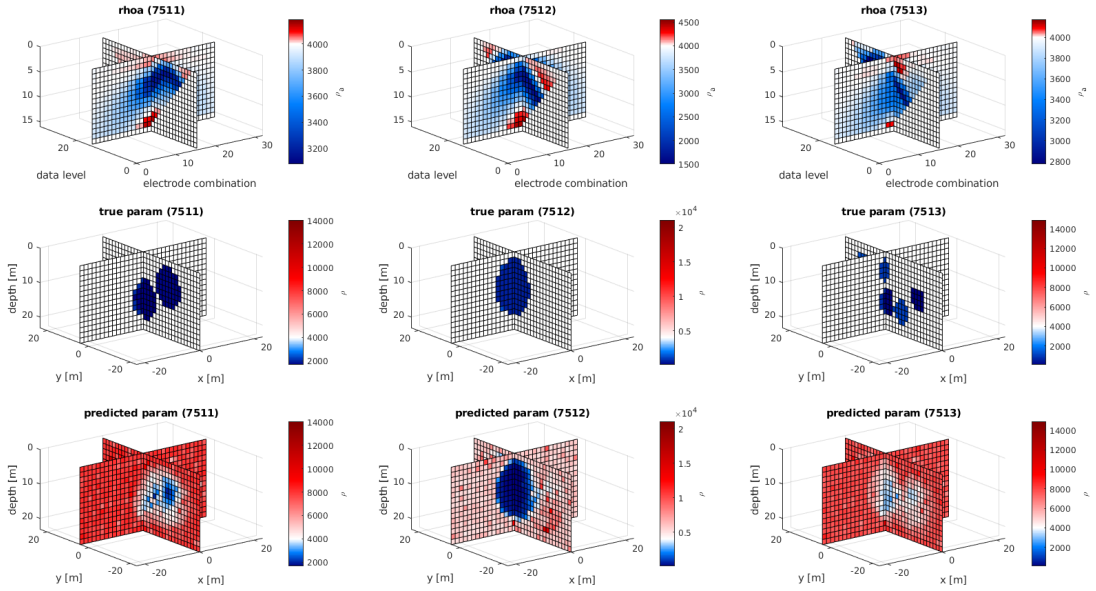

Figure 6: Training results for 3D data without noise. From top to bottom: Input ρ_a, ground truth (ρ), predicted ρ. From left to right represents 3 different cases.

4 Limitations

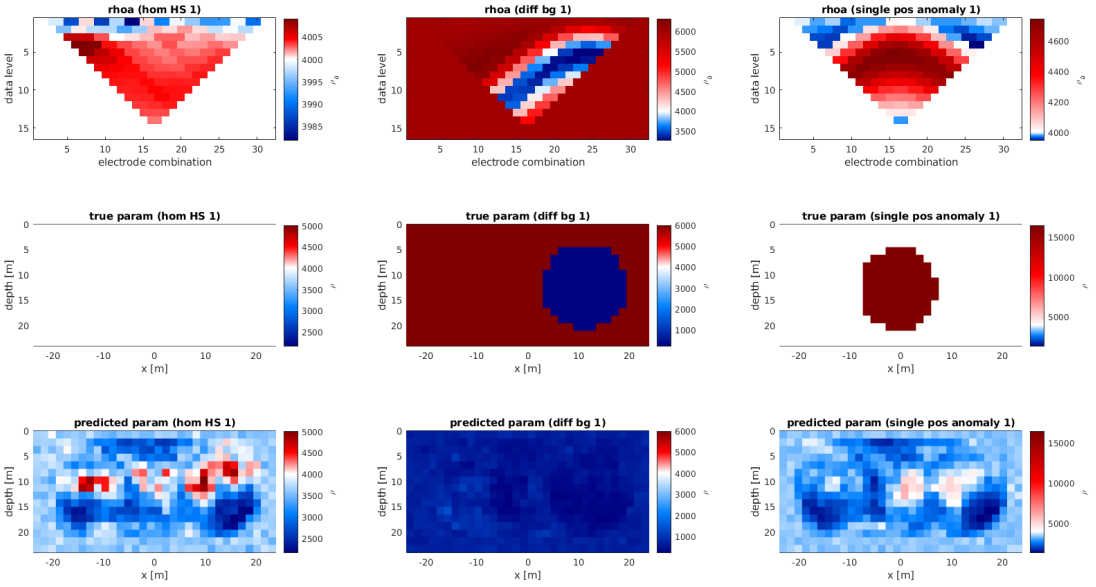

Figure 7: 2D evaluation of cases outside the scope of trained data. From top to bottom: Input ρ_a, ground truth (ρ), predicted ρ. From left to right: homogeneous half-space, higher background resistivity of $6000\Omega m$, higher resistive anomaly.

The presented approach is very limited in scope. Only cases with conductive anomalies were used for training. This means a fully learned network cannot predict cases outside of this scenario accurately. This can be seen in Fig. 7. The ground truth of all scenarios does not match the prediction. Cases such as homogeneous half-spaces and also bodies could potentially be added to the training pool. However, the case of higher background resistivity poses a particularly large problem, as training would have to be performed anew for every different geological situation.

5 Outlook

The presented approach is promising for a limited number of scenarios. However, as seen in the previous section, there are a number of limitations. Some of these can be overcome by more training with more varied types of data. However, the current approach requires setting a background resistivity. This poses a major problem for applicability, as the training would have to be redone for each new geologic situation. Without further developments, the current approach is thus not realistically suitable for the inversion of real world data. Different data transformations (to achieve the desired input shape from pseudo sections) could present an improvement. One possible application of this sort of approach lies in the generation of starting models for other inversion techniques.
Generally, an approach combining knowledge about the underlying physics and neural networks could prove most fruitful.

References

Abadi, M., Barham, P., Chen, J., Chen, Z., Davis, A., Dean, J., et al. (2016). Tensorflow: A system for large-scale machine learning. In *12th {USENIX} symposium on operating systems design and implementation ({OSDI} 16)* (pp. 265–283).

Badrinarayanan, V., Kendall, A., & Cipolla, R. (2017). Segnet: A deep convolutional encoder-decoder architecture for image segmentation. *IEEE transactions on pattern analysis and machine intelligence*, *39*(12), 2481–2495.

Ronneberger, O., Fischer, P., & Brox, T. (2015). U-net: Convolutional networks for biomedical image segmentation. In *International conference on medical image computing and computer-assisted intervention* (pp. 234–241).

Scheunert, M., Blechta, J., Börner, R.-U., Ernst, O., & Spitzer, K. (2021). Matlab FE library for simulation and inversion of EM problems. In J. H. Börner & P. Yogeshwar (Eds.), *Proceedings of the Schmucker-Weidelt Colloquium on Electromagnetics (this volume)*. Deutsche Geophysikalische Gesellschaft.

Vu, M., & Jardani, A. (2021). Convolutional neural networks with segnet architecture applied to three-dimensional tomography of subsurface electrical resistivity: Cnn-3d-ert. *Geophysical Journal International*, *225*(2), 1319–1331.